Method of compensating for pixel migration in volume holographic optical disc (VHOD)

Yeh-Wei Yu,[1] Chih-Yuan Cheng,[1] Tun-Chien Teng,[2] Cheng-Hsien Chen,[1]Shiuan-Huei Lin,[3] Bo-Rong Wu,[1] Che-Chih Hsu,[1] Yi-Jiun Chen,[1]Xuan-Hao Lee,[1] Chi-Yu Wu,[1] and Ching-Cherng Sun[1,*]

[1] *Department of Optics and Photonics, National Central University, Chung-Li 32001, Taiwan*
[2] *Department of Mechatronic Technology, National Taiwan Normal University, Taipei 10610, Taiwan*
[3] *Department of Electrophysics, National Chiao Tung University, Hsinchu 30050, Taiwan*
[*] *ccsun@dop.ncu.edu.tw*

Abstract: Volume holographic optical disc (VHOD) technology is simpler than the angular multiplexing holographic system. However, disc rotation usually causes pixel migration, thus reducing signal quality. This study proposes a special geometrical arrangement to counteract pixel migration. Using paraxial approximation analysis, an optimal geometrical distance ratio, *K*, is calculated to compensate for pixel migration and improve image quality during disc rotation. The results of approximation analysis are confirmed by both simulation and experimental results.

OCIS codes: (210.2860) Holographic and volume memories.

References and links

1. Digital Imaging and Communications in Medicine (DICOM), NEMA Standards Publications. *http://medical.nema.org/*.
2. K. D. Foord, "PACS workstation respecification: display, data flow, system integration, and environmental issues, derived from analysis of the Conquest Hospital pre-DICOM PACS experience," Eur. Radiol. **9**(6), 1161–1169 (1999).
3. J. Bernarding, A. Thiel, and A. Grzesik, "A JAVA-based DICOM server with integration of clinical findings and DICOM-conform data encryption," Int. J. Med. Inform. **64**(2-3), 429–438 (2001).
4. J. Fernàndez-Bayó, O. Barbero, C. Rubies, M. Sentís, and L. Donoso, "Distributing Medical Images with Internet Technologies: a DICOM Web Server and a DICOM Java Viewer," Radiographics **20**(2), 581–590 (2000).
5. R. N. J. Graham, R. W. Perriss, and A. F. Scarsbrook, "DICOM demystified: A review of digital file formats and their use in radiological practice," Clin. Radiol. **60**(11), 1133–1140 (2005).
6. IBM, "Tape storage systems," *http://www-03.ibm.com/systems/storage/tape/*.
7. P. J. van Heerden, "Theory of optical information storage in solids," Appl. Opt. **2**(4), 393 (1963).
8. A. Pu and D. Psaltis, "Holographic data storage with 100 bits/μm^2 density," Optical Data Storage Topical Meeting Conference Digest, 48–49 (1997).
9. G. W. Burr, C. M. Jefferson, H. Coufal, C. Gollasch, M. Jurich, J. A. Hoffnagle, R. Macfarlane, and R. M. Shelby, "Volume holographic data storage at an areal density of 100 Gbit/in^2," Conference on Lasers and Electro-Optics, 188–189 (2000).
10. N. Butt, K. Mcstay, A. Cestero, H. Ho, W. Kong, S. Fang, R. Krishnan, B. Khan, A. Tessier, W. Davies, S. Lee, Y. Zhang, J. Johnson, S. Rombawa, R. Takalkar, A. Blauberg, K. V. Hawkins, J. Liu, S. Rosenblatt, P. Goyal, S. Gupta, J. Ervin, Z. Li, S. Galis, J. Barth, M. Yin, T. Weaver, J. H. Li, S. Narasimha, P. Parries, W. K. Henson, N. Robson, T. Kirihata, M. Chudzik, E. Maciejewski, P. Agnello, S. Stiffler, and S. S. Iyer, "A 0.039 μm^2 High Performance eDRAM Cell based on 32nm High-K/Metal SOI Technology," IEEE International Electron Devices Meeting, 27.5.1 – 27.5.4 (2010).
11. L. Hesselink, S. Orlov, and M. Bashaw, "Holographic data storage systems," Proc. IEEE **92**(8), 1231–1280 (2004).
12. J. J. Amodei and D. L. Staebler, "Holographic pattern fixing in electro-optic crystals," Appl. Phys. Lett. **18**(12), 540–542 (1971).
13. F. Micheron and G. Bismuth, "Electrical control of fixation and erasure of holographic patterns in ferroelectric materials," Appl. Phys. Lett. **20**(2), 79–81 (1972).
14. D. von der Linde, A. M. Glass, and K. F. Rodgers, "Multiphoton photorefractive processes for optical storage in LiNbO3," Appl. Phys. Lett. **25**(3), 155–157 (1974).
15. D. Psaltis, K. Buse, and A. Adibi, "Non-volatile holographic storage in doubly doped lithium niobate crystals," Nature **393**(6686), 665–668 (1998).

#168221 - $15.00 USD Received 15 May 2012; revised 2 Aug 2012; accepted 5 Aug 2012; published 28 Aug 2012

16. F. Liu, Y. Kong, X. Ge, H. Liu, S. Liu, S. Chen, R. Rupp, and J. Xu, "Improved sensitivity of nonvolatile holographic storage in triply doped LiNbO3:Zr,Cu,Ce," Opt. Express **18**(6), 6333–6339 (2010).
17. K. Meerholz, B. L. Volodin, Sandalphon, B. Kippelen, and N. Peyghambarian, "A Photorefractive polymer with high optical gain and diffraction efficiency near 100%," Nature **357**, 479–500 (1994).
18. S. Tay, P.-A. Blanche, R. Voorakaranam, A. V. Tunç, W. Lin, S. Rokutanda, T. Gu, D. Flores, P. Wang, G. Li, P. St Hilaire, J. Thomas, R. A. Norwood, M. Yamamoto, and N. Peyghambarian, "An updatable holographic three-dimensional display," Nature **451**(7179), 694–698 (2008).
19. K. Curtis, L. Dhar, A. Hill, W. Wilson, and M. Ayres, *Holographic Data Storage: From Theory to Practical Systems* (Wiley, 2010).
20. G. Barbastathis, M. Levene, and D. Psaltis, "Shift multiplexing with spherical reference waves," Appl. Opt. **35**(14), 2403–2417 (1996).
21. H. Y. S. Li and D. Psaltis, "Three-dimensional holographic disks," Appl. Opt. **33**(17), 3764–3774 (1994).
22. T. C. Teng, Y. W. Yu, and C. C. Sun, "Enlarging multiplexing capacity with reduced radial cross talk in volume holographic discs," Opt. Express **14**(8), 3187–3192 (2006).
23. J. W. Goodman, *Introduction to Fourier Optics* (McGraw-Hill, 2002).
24. C. C. Sun, "Simplified model for diffraction analysis of volume holograms," Opt. Eng. **42**(5), 1184–1185 (2003).
25. G. P. Nordin and P. Asthana, "Effects of cross talk on fidelity in page-oriented volume holographic optical data storage," Opt. Lett. **18**(18), 1553–1555 (1993).
26. Members of the Technical Staff, Bell Laboratories, *Transmission Systems for Communications* (Bell Laboratories, Holmdel, N.J., 1971), Chap. 30, p. 726.
27. M. Born and E. Wolf, *Principles of Optics*, 6th ed. (Pergamon, New York, 1980), p. 382.

1. Introduction

In this era of information proliferation, the demands for efficient data back-up are growing quickly. This growth is driven by the rapid progress in digital technologies, e.g., super computers, global servers, and cloud computing. In addition, huge piles of data are produced by new imaging technologies such as high definition and three-dimensional imaging used by media companies and magnetic resonance imaging (MRI), computed tomography (CT), ultrasonic imaging (USI), and computed radiography (CR) used in hospitals [1–5]. The storage of these data presents many challenges. Generally, the relevant archives must be resistant to corruption, retrievable and operable at all times, expandable, and easy to store and manage. In addition, damaged or lost data must be recoverable, and the related hardware and software must be energy efficient and compact. Media companies and hospitals often have the further requirement that the databases be un-rewritable and unerasable.

Library-style tape storage systems have been used for archive [6]. However, the serial access of this method makes it too inefficient for many modern applications. On the other hand, the hard disk archive consuming too much electrical energy becomes heavy loading of big company. The best modern alternative is the volume holography storage system, which has a theoretical storage capacity as high as V/λ^3, with V being the recording volume and λ the wavelength of the recording light source [7]. The capacity of a volume holographic storage system is reported to be as high as 100 bits/μm^2 [8, 9]. Its densities are greater than those of even the latest 32 nm process dynamic random access memory (DRAM) [10], and because two-dimensional data arrays are recorded and retrieved at the speed of light, the page-based technique can transfer data at rates measured in GB/s [11]. Furthermore, multiphoton photorefractive processes and photorefractive polymers promise the rewritable-applications in the future [12–18].

The angular multiplexing holographic storage systems available commercially have high storage capacities and high transfer rates [19], but their mechanisms are intrinsically complex. Conversely, the shifting multiplexing of the spherical reference light in the so-called volume holographic optical disc (VHOD) system requires only that the disc be rotated [20, 21], simplifying and further compacting the mechanism. Nonetheless, two factors limit the application of VHOD. First, radial oriented inter-page cross-talk caused by Bragg degeneracy limits storage capacity (although this problem has recently been shown to be mitigated by introducing a spatial filter in the reference beam [22]). Second, the readout signal of the VHOD shifts when the disc rotates, resulting in extra inter-pixel crosstalk that decreases the signal-to-noise ratio (SNR). This study proposes a method for addressing these problems.

#168221 - $15.00 USD Received 15 May 2012; revised 2 Aug 2012; accepted 5 Aug 2012; published 28 Aug 2012

2. Theory

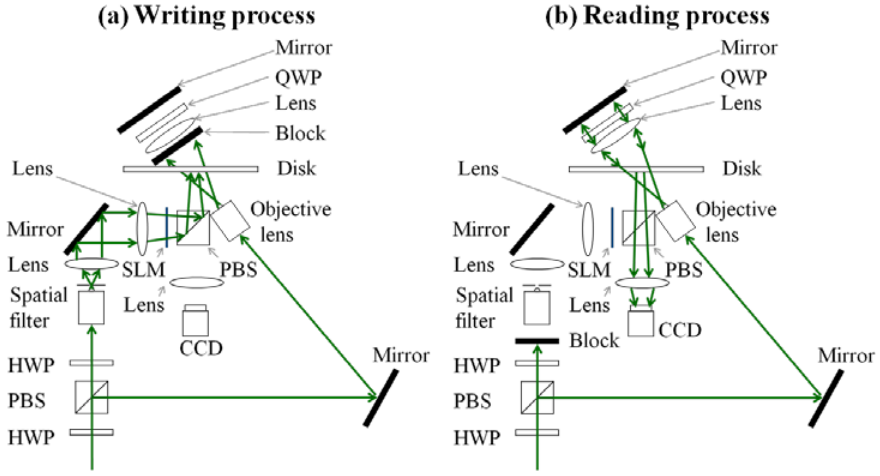

Fig. 1. Schematic outline of VHOD. (a) Writing process. (b) Reading process.

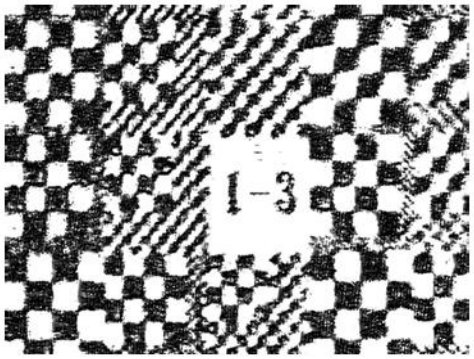

Fig. 2. Contrast enhanced image captured by the CCD in the reading process (Media 1).

Figure 1 shows the structure of the VHOD system. During the writing process, the signal beam consists of a convergent spherical wave that illuminates the spatial light modulator (SLM) and focuses on the disc. The interference between a divergent spherical reference (R) and the signal beam (S) is recorded. In the readout process, the conjugation of the reference (R*) serves as the reading light incident on the disc. Thus, the conjugation of the signal (S*) is diffracted and imaged on the CCD. Although simpler than traditional shifting multiplexing, by retaining the spherical-wave reference beam and recording the Fourier spectrum of the signal as before, VHOD suffers from the same problems of limited storage capacity and decreased SNR. Figure 2 (Media 1) shows a contrast enhanced image captured by the CCD in the reading process. The shift of the disc not only causes a corresponding shift of the diffracting signal, thus degrading the captured signal, but also leads to critical deviation tolerance. To solve the problem of pixel migration, we start from the theoretical model based on the VOHIL model and Fresnel diffraction [23, 24]. A schematic diagram of VHOD is shown in Fig. 3.

The reference distribution in the disc is a divergent spherical wave. By paraxial approximation and coordinate rotation, the reference can be expressed as

#168221 - $15.00 USD Received 15 May 2012; revised 2 Aug 2012; accepted 5 Aug 2012; published 28 Aug 2012

$$R_m\left(x_m, y_m, z_m\right) = \frac{1}{r}\exp\left\{ik\left(\frac{x_m{}^2 \cdot \cos^2\theta + z_m{}^2 \cdot \sin^2\theta - x_m \cdot z_m \sin 2\theta + y_m{}^2}{2r} + r\right)\right\}, \quad (1)$$

where (x_m, y_m, z_m) is the coordinate attached on the disc, k is the wave number, θ is the incident angle of the reference beam, and r is the distance from a given position inside the disc to the focus plane of the reference. The derivation of r is as follows:

$$r = r_0 + x_m \sin\theta + z_m \cos\theta, \quad (2)$$

where r_0 is the distance between the disc and the point source of the reference beam. The signal distribution inside the recording disc is

$$S_m\left(x_m, y_m, z_m\right) = \frac{\exp\left(ik\left(z_0 + z_m\right)\right)}{i\lambda\left(z_0 + z_m\right)}\exp\left(i\pi\frac{x_m{}^2 + y_m{}^2}{\lambda\left(z_0 + z_m\right)}\right)\iint S_0\left(x_s, y_s\right)\exp\left(i\pi\frac{x_s{}^2 + y_s{}^2 - 2x_s x_m - 2y_s y_m}{\lambda\left(z_0 + z_m\right)}\right)dx_s dy_s. \quad (3)$$

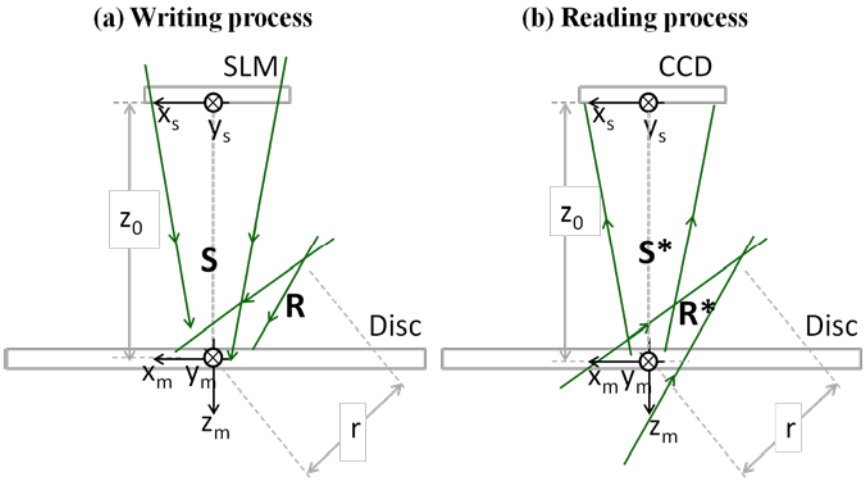

Fig. 3. Schematic diagram of VHOD. (a) Writing process. (b) Reading process.

where S_0 is the field distribution after modulation of the focusing signal beam by SLM, (x_s, y_s) are the coordinates attached on the SLM or CCD, z_0 is the distance between the disc and the SLM, and λ is the wave length.

The interfering fringe of the signal and the reference is

$$G_m = \left|R_m\right|^2 + \left|S_m\right|^2 + R_m{}^* S_m + S_m{}^* R_m, \quad (4)$$

Because the probing beam is the phase conjugation of the reference, only the last term is retrieved by the system, and we only consider

$$G_m = S_m{}^* R_m. \quad (5)$$

The phase conjugation of the reference reads the grating when the disc shifts (Δx, Δy), and the amplitude of the signal diffracting from each position inside the disc is

$$D_m\left(x_m, y_m, z_m\right) = circ\left(\frac{\sqrt{x_m{}^2 + y_m{}^2}}{w}\right)R_m{}^*\left(x_m, y_m, z_m\right)G_m\left(x_m - \Delta x, y_m - \Delta y, z_m\right), \quad (6)$$

#168221 - $15.00 USD Received 15 May 2012; revised 2 Aug 2012; accepted 5 Aug 2012; published 28 Aug 2012

where $circ\left(\frac{\sqrt{x_m^{\,2}+y_m^{\,2}}}{w}\right)$ stands for the system pupil with radius w. The amplitude of the diffracting signal propagating to the CCD is calculated by the Fresnel diffraction.

$$D_s(x_s,y_s,z_m)=\exp\left(i\frac{\pi\left(x_s^{\,2}+y_s^{\,2}\right)}{\lambda\left(z_0+z_m\right)}\right)\iint D_m(x_s,y_s,z_m)\exp\left(i\pi\frac{x_m^{\,2}+y_m^{\,2}-2x_sx_m-2y_sy_m}{\lambda\left(z_0+z_m\right)}\right)dx_m\,dy_m\,, \quad (7)$$

To obtain an analytical solution, we use the property

$$r_0 >> x_m \sin\theta. \quad (8)$$

The parameter r approximates as follows:

$$r \approx r_0 + z_m \cos\theta. \quad (9)$$

Therefore, we obtain the amplitude of the diffractive signal from depth z_m, as follows:

$$D_s(x_s,y_s,z_m)=F\cdot\left(S_p\otimes PSF\otimes Delta\right), \quad (10)$$

where

$$F(x_s,y_s,z_m)=\exp\left(\frac{i\pi}{\lambda}\left(\frac{x_s^{\,2}+y_s^{\,2}-\Delta x^2-\Delta y^2}{z_0+z_m}+\frac{\Delta x^2\cos^2\theta+\Delta y^2+\Delta x\cdot z_m\sin 2\theta}{r_0+z_m\cos\theta}-2\Delta x\sin\theta\right)\right), \quad (11)$$

$$S_p(x_s,y_s,z_m)=S_0^{\,*}(x_s,y_s)\exp\left(-i\pi\frac{x_s^{\,2}+y_s^{\,2}+2\Delta xx_s+2\Delta yy_s}{\lambda\left(z_0+z_m\right)}\right), \quad (12)$$

$$PSF(x_s,y_s,z_m)=\frac{\lambda\left(z_0+z_m\right)J_1\left(2\pi w\frac{\sqrt{x_s^{\,2}+y_s^{\,2}}}{\lambda\left(z_0+z_m\right)}\right)}{\pi w\sqrt{x_s^{\,2}+y_s^{\,2}}}, \quad (13)$$

and

$$Delta(x_s,y_s,z_m)=\delta\left(x_s-\Delta x\left(1-\frac{\left(z_0+z_m\right)\cos^2\theta}{r_0+z_m\cos\theta}\right),y_s-\Delta y\left(1-\frac{\left(z_0+z_m\right)}{r_0+z_m\cos\theta}\right)\right). \quad (14)$$

Each function has a unique physical property. The F function is a phase distribution; the S_p function is the mathematical product of a signal distribution and a phase distribution; PSF is a point spread function caused by the system pupil; and the Delta function describes the shift of the diffracting pattern. The Delta function is the key factor in the present analysis. When the disc rotates, the tangential shift (Δx) is greater than the radial shift (Δy). Therefore, if

$$\frac{r_0}{z_0}=\cos^2\theta, \quad (15)$$

Δx is multiplied by a number approaching zero in Eq. (14). In other words, the shift of the disc causes the smallest possible shift of the diffracting pattern. We use K to mean r_0/z_0:

$$K=\frac{r_0}{z_0}. \quad (16)$$

#168221 - $15.00 USD Received 15 May 2012; revised 2 Aug 2012; accepted 5 Aug 2012; published 28 Aug 2012

Described in physical terms, the solution of pixel migration is effectuated through displacement compensation. When the disc shifts, there is a corresponding positive shift of the recording position and a corresponding negative shift of the diffracting image. When the distance ratio equals $\cos^2\theta$, the positive and negative shifts compensate for each other. Thus, the pixel migration is resolved.

3. Simulation

Using Eq. (7), a simulation can be conducted based on the Fresnel diffraction and the VOHIL theorem (the approximation in Eq. (9) is not used). By integrating D_s along depth z_m, we obtain the intensity distribution in the CCD plane.

$$I_{CCD}(x_s, y_s) = \left| \int_{-\frac{T}{2}}^{\frac{T}{2}} D_s(x_s, y_s, z_m) dz_m \right|^2 . \tag{17}$$

In the simulation, the thickness of the disc is 1.8 mm and the refractive index is 1.5. The wavelength inside the disc is 0.532/1.5 μm. The effective incident angle of the reference is 15°. The effective distance, r_0, is kept at 40 mm to keep the same shift selectivity. z_0 is 20 mm for $K = 2$ and 42.9 mm for $K = \cos^2\theta$. The signal in the SLM is 50 × 50 pixels with randomly distributed 0's and 1's. The pixel-number ratio between 0's and 1's is 1:1. The pixel size of

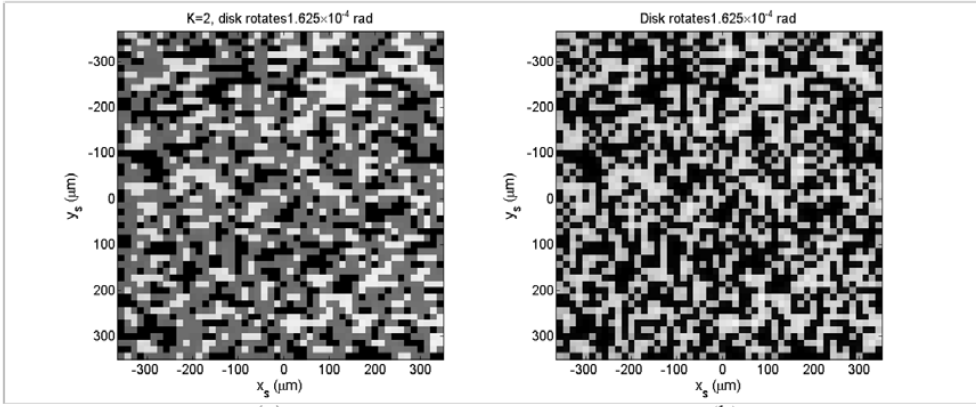

Fig. 4. Diffracted signal captured by the CCD. (a) K = 2 (Media 2). (b) K = $\cos^2\theta$(Media 3). both the SLM and the CCD is 14 × 14 μm^2. Figure 4(a) (Media 2) and Fig. 4 (b) (Media 3) show the diffracting signal captured by the CCD when $K = 2$ and $K = \cos^2\theta$, respectively. As expected, the diffracting signal in Fig. 4(a) (Media 2) shifts, but that in Fig. 4 (b) (Media 3) remains steady. Figure 4 (b) (Media 3) consequently shows greater image quality when the disc rotates. The SNRs were calculated according to the following formula:

$$SNR = 20 \cdot \log\left\lfloor \frac{(m_1 - v_{th})}{\sigma_1} \right\rfloor, \tag{18}$$

where m_1 and m_0 are the means of the distribution of 1's and 0's, respectively [25, 26]. σ_1 and σ_0 are the standard deviations of the distribution of 1's and 0's, respectively. v_{th} is the threshold value between the 1's and the 0's, and is calculated as follows:

$$v_{th} = \frac{\sigma_1 m_0 + \sigma_0 m_1}{\sigma_1 + \sigma_0}, \tag{19}$$

Figure 5 shows the SNR of the diffracting signal plotted against the disc rotation. The blue and red curves stand for $K = 2$ and $K = \cos^2\theta$, respectively. With the disc in the initial position

#168221 - $15.00 USD Received 15 May 2012; revised 2 Aug 2012; accepted 5 Aug 2012; published 28 Aug 2012

in the writing process, the blue curve is higher than the red curve because the smaller z_0 yields a greater point spread function. However, as the disc falls out of precise alignment, the blue curve drops considerably faster than the red curve. In other words, pixel migration has been avoided at the price of a slight decrease in SNR.

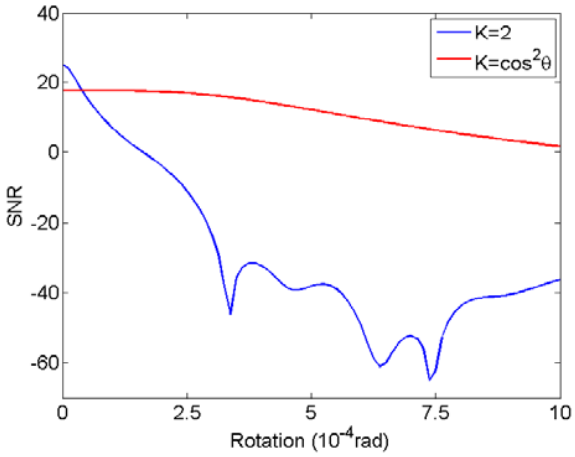

Fig. 5. SNR of diffracting signal depending on disc rotation.

4. Experiment

Figure 6 shows the experimental apparatus used to demonstrate this technique. Its setup is the same as that shown in Fig. 1, except that an additional CCD B is used to capture diffracting signals (S). The light source is a Verdi-laser with a wavelength of 0.532 μm. The signal beam is a convergent spherical wave illuminating the SLM and focusing on the disc. The disc is positioned near the focus of the signal beam but deviates slightly from the focus depth to avoid a strong DC term.

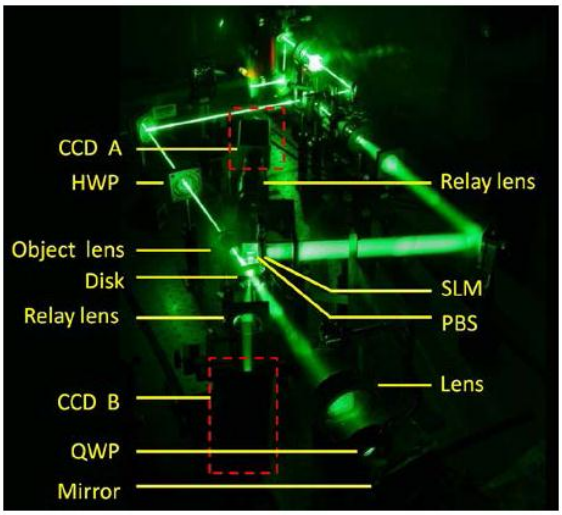

Fig. 6. The experimental setup.

The recording medium is a PQ/PMMA photopolymer 1.8 mm in thickness. The refractive index of the PQ/PMMA is 1.5. The signal beam normally strikes the disc with a distance of 6.8 cm between the SLM and the disc. Because of the refractive boundary, the effective distance inside the disc is 10.2 cm. The reference beam is a divergent spherical wave with an

#168221 - $15.00 USD Received 15 May 2012; revised 2 Aug 2012; accepted 5 Aug 2012; published 28 Aug 2012

incident angle of 22.8°, which corresponds to 15° inside the disc. The distance from the divergent point of the reference to the recording region on the disc is 6.4 cm. From the geometric schematic diagram shown in Fig. 7, we obtain

$$r_{air}\sin(23.3^{\circ}) = r_{disk}\sin(15^{\circ}). \tag{20}$$

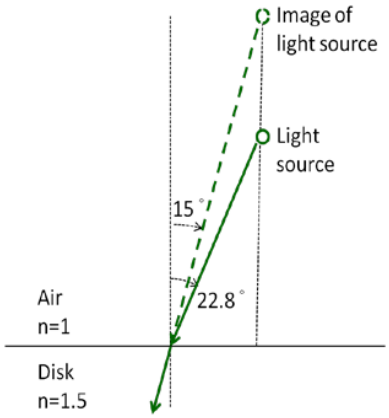

Fig. 7. Schematic diagram for position of effective light source.

The resulting effective distance inside the disc (r_{disc}) is 9.5 cm. The K factor thus equals $\cos^2\theta$ and fits Eq. (15). In the readout process, the conjugation of the reference (R*) serves as the reading light. Thus, the conjugation of the signal (S*) is diffracted and imaged on CCD A. The contrast enhanced image in Fig. 8 (Media 4) shows that when the disc shifts, the diffracting image dims but remains in the same position. Compared to Fig. 2 (Media 1), the improvement is evident.

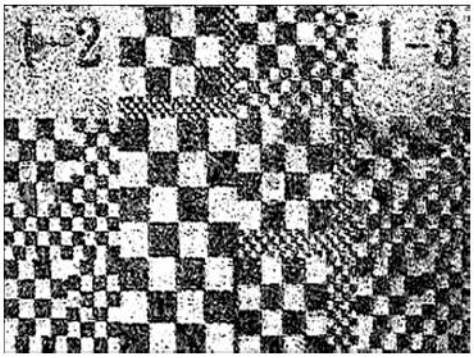

Fig. 8. Contrast enhanced image captured by the CCD in the reading process (Media4).

5. Application

Using an optimal value for *K*, the signal can be read even when the disc continues to rotate. In the simulation, we accumulated the signal with the disc rotating from 0 rad to 10^{-3} rad (Fig. 9). Figure 9(a) (Media 5) and Fig. 9(b) (Media 6) show the accumulated signals when $K = 2$ and $K = \cos^2\theta$, respectively, and show how the image quality in Fig. 9(b) (Media 6) remains relatively unchanged as the disc rotates. Figure 10 shows the SNR plotted against disc rotation. The horizontal axis is the accumulation distance, and the blue and red curves stand for $K = 2$ and $K = \cos^2\theta$, respectively. Significantly, the red curve remains above 10 throughout the range of accumulated distance from 0 rad to 10^{-3} rad, reflecting the degree to

#168221 - $15.00 USD Received 15 May 2012; revised 2 Aug 2012; accepted 5 Aug 2012; published 28 Aug 2012

which the data transfer rate is enhanced by the ability to read the signal while the disc is rotating.

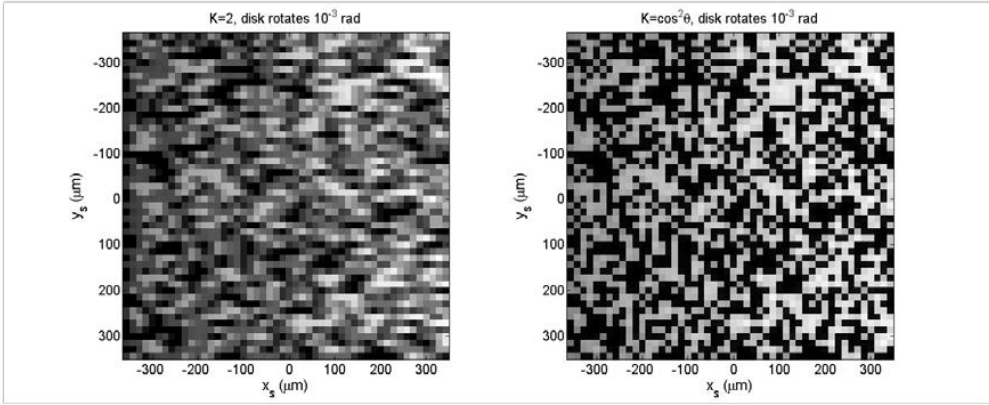

Fig. 9. Accumulated signal with disc rotating from 0 rad to 10^{-3} rad. (a) K = 2 (Media 5). (b) K = $\cos^2\theta$ (Media 6).

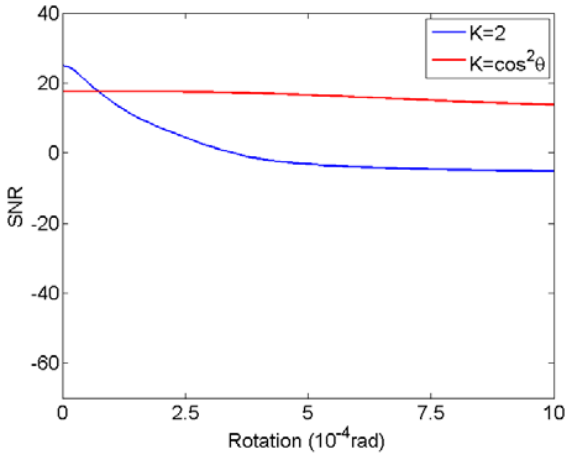

Fig. 10. SNR depending on disc rotation.

6. Analysis for SLM with wide area

Equation (15) is derived out based on paraxial condition. Nevertheless, the system is composed of a SLM with wide area and a reference with a divergent beam. So, the geometric relationship described by Eq. (15) can't be satisfied for signal in any position of the SLM. Here, we analyze the applicability of compensating pixel migration for signal in different locations. The Rayleigh-Sommerfeld diffraction theory is used in order to simulate light propagating at large angle [27]. Figure 11 shows the schematic diagram for both $K = \cos^2\theta$ and $K = 2$. The parameters are the same as other simulations in this paper except the dimension of the SLM. The width of SLM in x direction is 28mm, corresponding to 2000 pixel numbers. θ_s is the inclined angle of the light when it propagates from the signal to the focus point. The simulation results for SNR depending on disc rotation among different θ_s range are shown in Fig. 12. In each case, 100 × 10 pixels are used as signal for $K = \cos^2\theta$, and pixels inside the same range of θ_s are used as signal for K = 2. The simulation results show the SNR drops down for large θ_s. Even so, the performance for K = $\cos^2\theta$ is always better than $K = 2$.

#168221 - $15.00 USD Received 15 May 2012; revised 2 Aug 2012; accepted 5 Aug 2012; published 28 Aug 2012

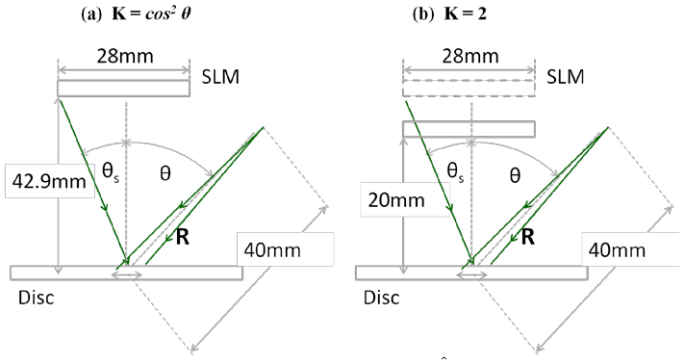

Fig. 11. Schematic diagram for (a) $K = \cos^2\theta$ and (b) $K = 2$.

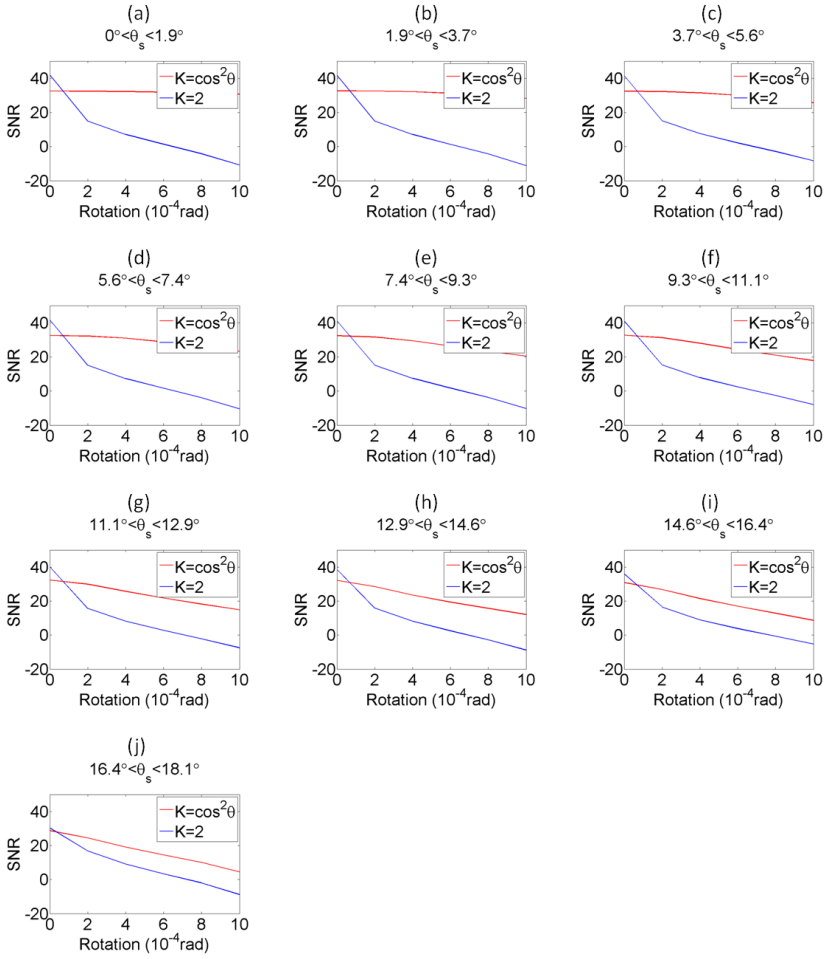

Fig. 12. SNR depending on disc rotation forθ_s in different range. (a) $0°<\theta_s<1.9°$. (b) $1.9°<\theta_s<3.7°$. (c) $3.7°<\theta_s<5.6°$. (d) $5.6°<\theta_s<7.4°$. (e) $7.4°<\theta_s<9.3°$. (f) $9.3°<\theta_s<11.1°$. (g) $11.1°<\theta_s<12.9°$. (h) $12.9°<\theta_s<14.6°$. (i) $11.1°<\theta_s<12.9°$. (j) $12.9°<\theta_s<14.6°$.

#168221 - $15.00 USD Received 15 May 2012; revised 2 Aug 2012; accepted 5 Aug 2012; published 28 Aug 2012

7. Conclusion

VHOD storage is simpler and more compact than angular multiplexing holographic storage. However, disc rotation typically causes pixel migration and a consequent decline in signal quality. This study proposed a geometrical algorithm to avoid pixel migration during the reading process. By making a paraxial approximation of VHOD, a geometrical distance ratio, *K*, can be calculated. When *K* equals $\cos^2\theta$, the system achieves displacement compensation, and the pixel migration is compensated for. This technique was demonstrated in a simulation video in which the SNR was used to assess diffracting signal quality. The video shows that with the disc in the initial writing position, there is no improvement at $K = \cos^2\theta$ because the relatively small z_0 induces a greater point spread function. However, when the disc is not aligned precisely, the SNR for K = 2 drops substantially faster than that for $K = \cos^2\theta$, indicating that the problem of pixel migration has been solved at the price of a slight decrease in SNR. An experiment to demonstrate the technique showed that when the disc shifted at $K = \cos^2\theta$, the diffracting image dimmed but remained in the same position. Compared to the results obtained with K = 2, the progress is evident. Thus, the technique of reading signals during disc rotation enhances the data transfer rate significantly. In the end, we check the performance of the system for signal with large size by Rayleigh-Sommerfeld diffraction theory. Although the simulation results show the SNR drops down for large θ_s, the performance for $K = \cos^2\theta$ is always better than $K = 2$.

Acknowledgment

This study was sponsored by the National Science Council of the Republic of China with the contracts of no. 97-2221-E-008-025-MY3, 99-2623-E-008-002-ET and NSC100-3113-E-008-001.

#168221 - $15.00 USD Received 15 May 2012; revised 2 Aug 2012; accepted 5 Aug 2012; published 28 Aug 2012